International Journal of Sciences and Techniques of Automatic control & computer engineering
IJ-STA, Volume 4, N° 2, December 2010, pp. 1320-1337.

Sensorless Sliding Mode Control of Induction Motor Pump fed by Photovoltaic Generator

Mohamed Abdellatif Khalfa [1,2], Anis . Sellami[1,2] and Radhi M'hiri[3]

[1]Research and Technologies of Energy Center, BorjCedria Technopark, Tunisia
[2]Unit of research: C3S. ESSTT, Tunis - Tunisia
Lotfi.Khalfa@isetn.rnu.tn, anis.sellami@esstt.rnu.tn
[3]FST University Campus 2092 Tunis El Manar
radhi.mhiri@yahoo.fr

Abstract. *This paper deals with the modeling and nonlinear sliding mode control with observer of a centrifugal pump system driven by a three-phase induction motor, which is supplied by a photovoltaic generator (PVG). This work is motivated by the need to track the maximum power from the PVG which is a non-linear device having illumination-dependent volt-ampere characteristic. This objective is reached by the application of a sliding mode control approach (SMC). First, the different models of elements composing the whole system are presented: the PVG, the DC/AC inverter, the induction motor (IM) and the pump. Second, we propose a sliding mode control which insures the convergence of the rotor speed and the square of the rotor flux magnitude to their references. This choice allows the PVG to work at its maximum power point. The obtained simulation results illustrate the validity and the performances of the suggested approach.…*

Keywords. *Sliding Mode Control; Photovoltaic Pumping System; Maximum Power Point Tracking; High Gain Observer; Induction Motor.*

1. Introduction

During the last decades, an effort has been focused on the use of solar energy. This energy, no polluting, available around the world, is certainly a suitable source for many applications such as: industrial and aero-spatial, domestic use in rural areas, desalination plants etc. Global warming due to emission of CO_2 and the shortness of fossil sources encouraged scientists to develop the field of renewable energy and specially the photovoltaic applications.

This paper was recommended for publication in revised form by the editor Staff.
Edition: CPU of Tunis, Tunisia, ISSN: 1737-7749

This paper deals with a photovoltaic pumping system without battery. This solution is more economic and friendly with environment due to elimination of the battery and his circuit of charge. The electric energy storage is replaced by a water storage in elevated tank witch can be used for a many purposes.

Direct coupling photovoltaic (PV) pumping system is characterized by a low yield. In order to improve the efficiency of the total system, PV generator is coupled to the pumps via power electronics interface. This electronic adapter is able to extract the maximum power point from PV generator, which depends on the load, the irradiance and the temperature. For this purpose, many algorithms are presented in the literature [1], [2], [4] and [7]: Hill Climbing, and perturb and observe (P&O), incremental conductance (IncCond), Fractional Open-Circuit Voltage, Fractional Short-Circuit Current etc. In this paper we adopted the P&O method. The induction motor occupies a very significant field in industry and transport. It is appreciated for its robustness, its low cost of purchase and maintenance. However, its control is more difficult to realize than other electric machines. Many strategies were developed to make of it a machine which exceeds the others, even in the controlled systems. In general, the control of the induction machine is divided into two classes:

- low cost control and weak performance (for example the *V/f* control)
- High performance control with a reasonable cost (for example sliding mode control which ensures a high dynamics…)

In this paper, a sliding mode control of a photovoltaic pumping system driven by a three-phase induction motor is proposed. This new developed approach insures the convergence of the rotor speed and the square of the rotor flux magnitude to their references, which allows the PV generator to work at its maximum power point.

The paper is organized as follows: section 1 presents an introduction. Section 2 deals with the modeling of the global system (PV generator and the maximum power point tracking problem, the three-phase inverter, induction motor pump). Section 3 presents the sliding mode control design. Section 4 deals with observer design. Finally, in section 5, some simulation results are given to validate the proposed control approach.

2. Photovoltaic Pumping System Description

The figure 1 shows the proposed structure of the PV pumping system.

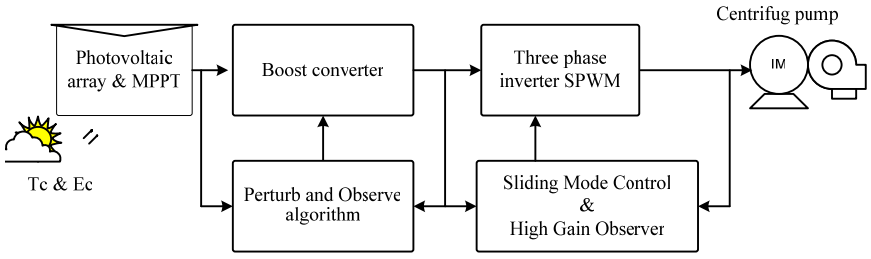

Fig. 1. Block diagram of photovoltaic pumping system

2.1. Photovoltaic Generator Modeling

The electric PV module equivalent circuit is shown in Fig. 2 [5], a single-diode model SDM from [6].

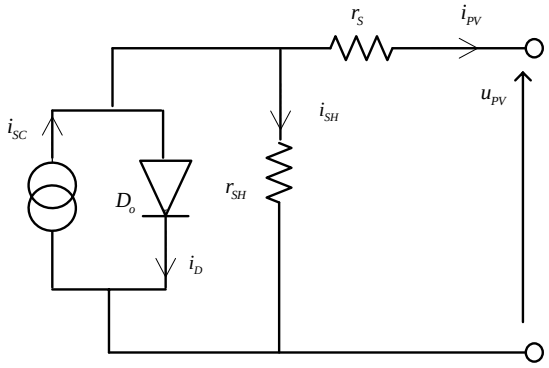

Fig. 2. The electric PV cell/module single-diode model.

The characteristic equation for the current and voltage of PV module is given as follows [7].

$$i_{PV,STC} = i_{SC,STC}\left[1 - K_1\left[\exp\left(K_2 u^{m}_{u_{PV,STC}}\right) - 1\right]\right] \quad (1)$$

With K_1, K_2, K_3, K_4 and m constants calculated independently of weather conditions.

$$K_1 = 0.01175;\ K_4 = \ln\left(\frac{1+K_1}{K_1}\right);$$
$$K_3 = \ln\left(\frac{i_{SC,STC}\,(1+K_1) - i_{MPP,STC}}{K_1\, i_{SC,STC}}\right);$$
$$m = \frac{\ln\left(\frac{K_3}{K_4}\right)}{\ln\left(\frac{u_{MPP,STC}}{u_{OC,STC}}\right)};\ K_2 = \frac{K_4}{u_{OC,STC}^{m}} \qquad (2)$$

The PV module used in this system is the SIEMENS SP-150, having the characteristics listed in Table I.

Table 1. Characteristics of the used solar module *SP150*	
Electrical parameters in Standard Test conditions *STC* [1)]Wp (Watt peak) = Peak power; Air Mass *AM= 1.5*; Irradiance E_{STC}= *1000 W/m2*; Cell temperature T_{STC}= 25 °C	
Maximum power rating $p_{MPP,STC}$	150 [Wp][1)]
Rated current $i_{MPP,STC}$	4.40 [A]
Rated voltage $u_{MPP,STC}$	34.0 [V]
Short circuit current $i_{SC,STC}$	4.80 [A]
Open circuit voltage $u_{OC,STC}$	43.4 [V]
Nnumber of cells in one panel N_{CSM}	72 pcs.
PV panel connection resistance r_S	35 [mΩ]
Thermal parameters [2)] Normal Operating Cell Temperature at: Irradiance *E= 800 W/m²* Ambient temperature $T_{A,REF}$ *= 20 °C* ; Wind speed v_W*= 1 m/s*	
NOCT[2)]	45±2 [°C]
Temp. coefficient of the short-circuit current α_{isc}	2.06[mA/°C]
Temp. coefficient of the open-circuit voltage α_{uoc}	-0.077 [V/°C]

The expression (1) generates $i_{PV,STC}$ ($u_{PV,STC}$) characteristic in the *STC*. For other values of illumination and temperature, the new current and voltage values of the PV panel are [7-8].

$$\Delta T = T_C - T_{STC} \quad \text{With} \quad T_C = T_A + \frac{E_C}{800}\left(NOCT - T_{A,REF}\right) \qquad (3)$$

$$\Delta i_{PV} = \alpha_{iSC} \frac{E_C}{E_{STC}} \Delta T + \left(\frac{E_C}{E_{STC}} - 1 \right) i_{SC,STC} \quad (4)$$

$$i_{PV} = i_{PV,STC} + \Delta i_{PV} \quad (5)$$

$$\Delta u_{PV} = -\alpha_{uoc} \Delta T - r_s \Delta i_{PV} \quad (6)$$

$$u_{PV} = u_{PV,STC} + \Delta u_{PV} \quad (7)$$

For a PVG made up of N_{BPG} branches in parallels, each branch is made up of N_{MSB} modules in series comprising in N_{CSM} cells in series [3]. The current delivered by the PVG and the corresponding voltage are:

$$\begin{cases} I_{PV} = N_{BPG}\ i_{PV} \\ U_{PV} = N_{MSB}\, u_{PV} \end{cases} \quad (8)$$

The PVG is formed with ten PV modules, which are connected with eight modules in series and two in parallel. Thus, the PVG have a peak output power of 1500W, an open-loop output voltage of 434 V, a short-circuit current of 4.8 A, and a peak current of 4.4 A at the peak power point.

2.2. The DC/ DC Boost Converter Model

DC-DC converters, as voltage elevators, are also used in PV applications, especially in PV pumping. The model of the DC/DC boost converter is obtained by application of basic laws governing the operation of the system. A boost converter is a power converter with an output DC voltage greater than its DC input voltage. It is a class of switching-mode power supply SMPS containing at least two semiconductor switches (a diode D and The switch Q is typically a MOSFET, IGBT, or BJT) an input filter (C_{PV}, L_{EH}) and an output filter C_{SH} [9]. The basic circuit is illustrated in figure 3.

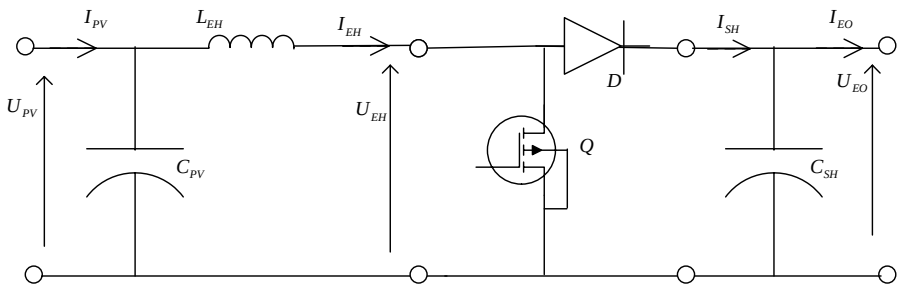

Fig. 2. The DC-DC Boost converter basic circuit.

The basic principle of a Boost converter consists in two distinct states:

- When the switch Q is ON, the current through the inductor L_{EH} increases and the energy stored in the inductor builds up;
- When the switch Q is off, current through the inductor continues to flow via the diode D, the C_{SH} network and back to the source.

The dynamics of this converter operating in the continuous conduction mode can be easily obtained by applying Kirchhoff laws.

$$\begin{cases} L_{EH}\dfrac{dI_{EH}}{dt}+U_{EH}=U_{PV} \\ C_{PV}\dfrac{dU_{PV}}{dt}=I_{PV}-I_{EH} \end{cases} \tag{9}$$

The time period is:

$$T=t_{ON}+t_{OFF} \tag{10}$$

The switch state is also governed by a control signal with a constant period T and a variable duty cycle α.

$$\begin{cases} \alpha=\dfrac{t_{ON}}{t_{ON}+t_{OFF}} \\ \dfrac{U_{SH}}{U_{EH}}=\dfrac{I_{EH}}{I_{SH}}=\dfrac{1}{1-\alpha} \end{cases} \tag{11}$$

Other hand, the output filter C_{SH}

$$C_{SH}\frac{dU_{SH}}{dt}=I_{SH}-I_{EO} \tag{12}$$

2.3. The MPPT Based on a DC/DC Boost Converter

Up to now, a number of MPPT algorithms have been proposed in the literature, including perturb-and observe method (P&O) [10-11], open- and short-circuit method [12], incremental conductance algorithm [13], fussy logic [14] and artificial neural network [15].

The P&O method, also known as perturbation method, is the most commonly used MPPT algorithm in commercial PV products [17-18]. P&O method has a simple feedback structure and fewer measured parameters. It operates by periodically perturbing (incrementing or decreasing) the array terminal voltage and comparing the PV output power with that of the previous perturbation cycle.

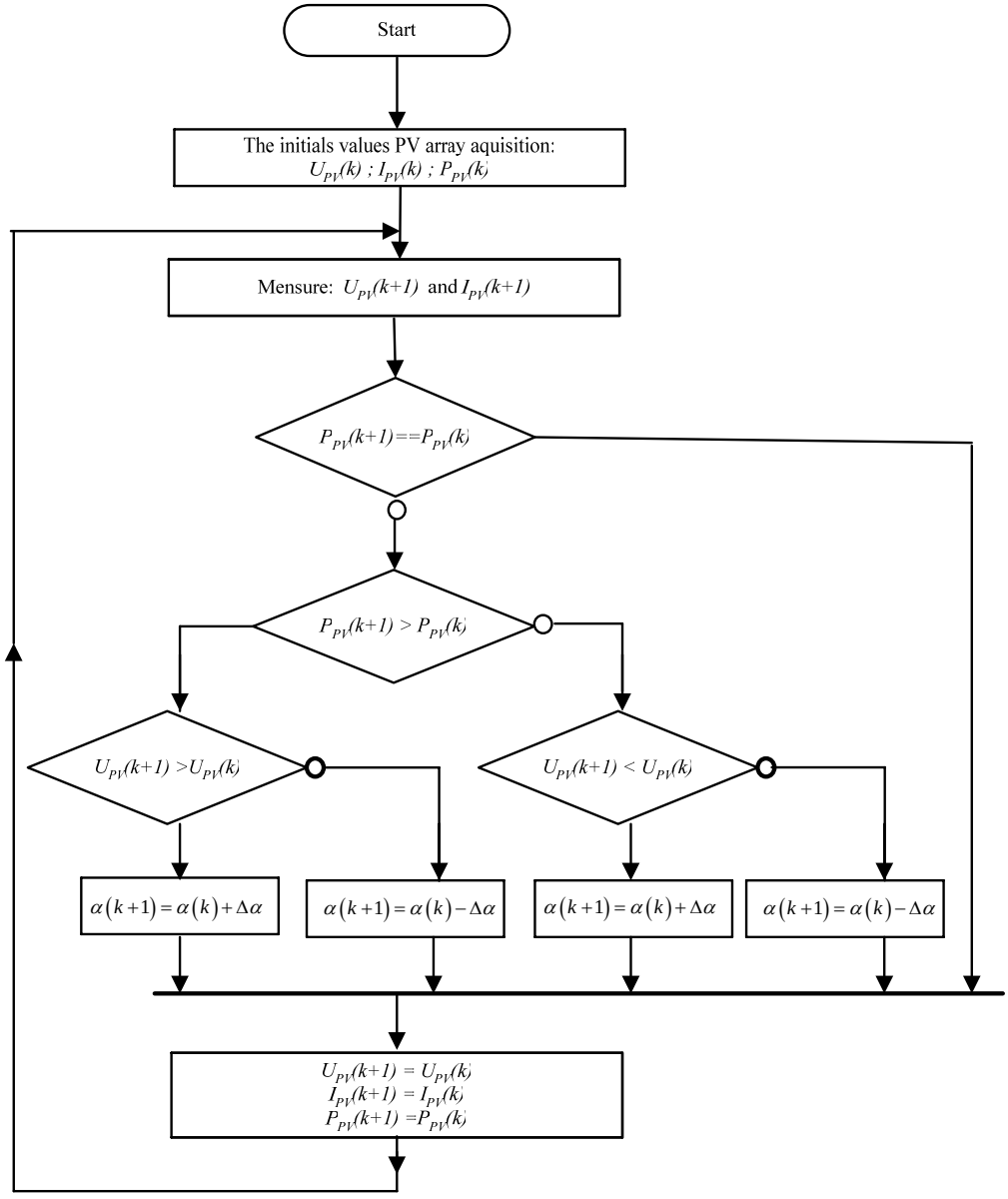

Fig. 4. The perturb and observe algorithm flowchart

The principle of this controller is to generate a perturbation by decreasing or increasing the PWM duty cycle and observing its effect on the output PV power [17–18]. If the instant power $P_{PV}(k+1)$ is greater than the previous computed power $P_{PV}(k)$, then

the direction of perturbation is maintained. Otherwise, it is reversed. Referring to Fig. 5, [2] this can be detailed as follows:

- When $dP_{PV}/dU_{PV} > 0$, the voltage is increased through $\alpha(k+1)= \alpha(k)+\Delta\alpha$,
- When $dP_{PV}/dU_{PV} < 0$, the voltage is decreased through $\alpha(k+1) = \alpha(k) -\Delta\alpha$.

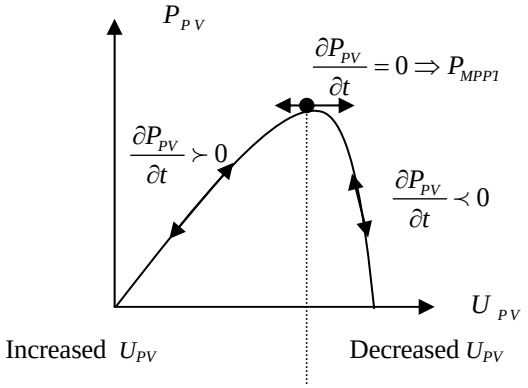

Fig. 3. The Power – Voltage characteristic [2]

2.4. The Modeling of PWM Three Phases Inverter

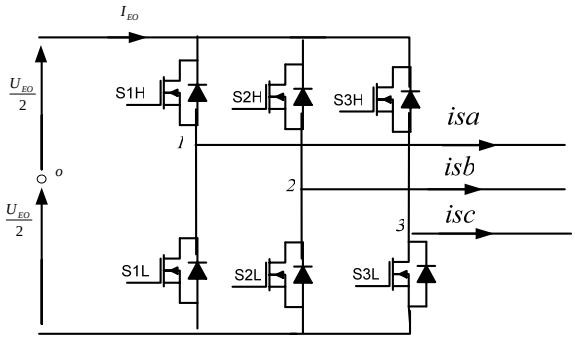

Fig. 5. The three phase inverter SPWM circuit

The most common method of control used today compares the voltage commands for each phase with a single triangle waveform. The commands could be derived from three individual phase voltage regulators. The electronic components are assumed to be perfect (instantaneous commutation, no voltage drop at conducting state).

The three-phase inverter consists of three independent arms including each one two switches. Each switch is composed of a transistor (IGBT, MOSFET…) and of a diode

coupled in parallel. The relation of the inverter input and output currents are given by the following expression:

$$i_{EO} = i_{sa}\ S_{1H} + i_{sb}\ S_{2H} + i_{sc}\ S_{3H} \tag{13}$$

The switches of each inverter arm are complementary; it is the same for the associated control signals. Thus we obtain:

$$S_{1L} = 1 - S_{1H} \quad S_{2L} = 1 - S_{2H} \quad S_{3L} = 1 - S_{3H} \tag{14}$$

Where

$$S_i = \begin{cases} 1 \rightarrow S_{iH} : on, S_{iL} : off \\ 0 \rightarrow S_{iH} : off, S_{iL} : on \end{cases} \tag{15}$$

The stator is connected as a three-wire system; hence:

$$u_{sa} + u_{sb} + u_{sc} = 0 \tag{16}$$

The following voltage equations may be written by using Fig. 6:

$$\begin{bmatrix} u_{sa} \\ u_{sb} \\ u_{sc} \end{bmatrix} = \frac{u_{EO}}{3} \begin{bmatrix} 2 & -1 & -1 \\ -1 & 2 & -1 \\ -1 & -1 & 2 \end{bmatrix} \begin{bmatrix} S_{1H} \\ S_{2H} \\ S_{3H} \end{bmatrix} \tag{17}$$

2.5. The Induction Motor Pump Model

In a two-phase (d-q) Park reference turning at synchronism speed $\omega_{dq}=\omega_s$, the mathematical model of the induction motor-pump in transient state is written in nonlinear equation forms as [3], [5] and [8].

$$\dot{X}(t) = A(X, t) + B(X)U \tag{18}$$

The vector of control $U=[u_{sd}\ u_{sq}]^T$; The vector of state is $X=[i_{sd}\ i_{sq}\ \varphi_{rd}\ \varphi_{rq}\ \omega]$, where:

u_{sd} , u_{sq}: the direct and quadrature stator voltages; i_{sd}, i_{sq} : the stator direct and quadrature axis currents in synchronously rotating reference frame; φ_{rd} φ_{rq}: the rotor direct and quadrature flux and ω the rotor angular speed in electrical radians per second.

$$\begin{cases} \dot{i}_{sd} = a_1\ i_{sd} + a_2\ i_{sq} + a_3\ \varphi_{rd} + a_4\ \varphi_{rq}\ \omega + b_1\ \ u_{sd} \\ \dot{i}_{sq} = -a_2 i_{sd} + a_1\ \varphi_{rd} - a_4 \omega \varphi_{rd} + a_3\ \varphi_{rq} + b_1\ \ u_{sq} \\ \dot{\varphi}_{rd} = a_5\ i_{sd} + a_6 \varphi_{rd} + (a_2 - \omega)\ \varphi_{rq} \\ \dot{\varphi}_{rq} = a_5\ i_{sq} - (a_2 - \omega) \varphi_{rd} + a_6\ \varphi_{rq} \\ \dot{\omega} = a_7 \left(\varphi_{rd} i_{sq} - \varphi_{rq} i_{sd}\right) + a_8 \left(C_r + C_f\right) \end{cases} \tag{19}$$

with:

$$a_1 = -\left(\frac{1}{\sigma\,\tau_s} + \frac{1-\sigma}{\sigma\,\tau_r}\right);\ a_5 = \frac{M_{sr}}{\tau_s};\ b_1 = \frac{1}{\sigma\,L_s};\ a_2 = \omega_{dq};\ a_6 = -\frac{1}{\tau_r};$$

$$\sigma = 1 - \frac{M^2_{sr}}{L_s L_r};\ a_3 = \frac{1-\sigma}{\sigma\,M_{sr}\,\tau_r};\ a_7 = \frac{3}{2}\frac{n_{pp}{}^2}{J}\frac{M_{sr}}{L_r};\ \tau_s = \frac{L_s}{R_s};\ a_4 = \frac{1-\sigma}{\sigma\,M_{sr}}; \quad (20)$$

$$a_8 = -\frac{n_{pp}}{J};\ \tau_r = \frac{L_r}{R_r};\ \omega = n_{pp}\,\Omega;\ \omega_s = 2\,\pi\,f_s$$

R_s, R_r: the rotor and stator winding resistances respectively; M_{sr} : the mutual inductance between rotor and stator windings; L_r , L_s: the rotor and stator self-inductances respectively; n_{pp} : the number of pole pairs; J : the rotor moment of inertia; C_r the resistive torque; C_f is the viscous friction torque; σ the total dispersion coefficient; τ_s the stator constant time; τ_r the rotor constant time ; n the rotor mechanical speed in [rpm]; Ω the angular rotor speed in [rad/s] ; ω the rotor electric speed; the stator electrical synchronism speed; the electromagnetic torque expression using rotor flux and the stator currents is

$$C_{ém} = \frac{3}{2}\,n_{pp}\,\frac{M_{sr}}{L_r}\left(\varphi_{rd}\ i_{sq} - \varphi_{rq} i_{sd}\right) \quad (21)$$

3. Nonlinear Sliding Mode Control Design

The approach proposed in this paper, is a nonlinear order based on the theory of systems with variable structure with sliding mode. In this part, our objective is to design a control law to drive the motor states to a properly designed sliding surface ensuring speed and flux references tracking [8]. The switching function considered a vector of the errors of electric speed of rotor ω and of the square of the rotor module of flux ϕ.

$$\phi = \varphi_{rd}^2 + \varphi_{rq}^2 \quad (22)$$

The switching function is given by [8].

$$\left.\begin{vmatrix} \varepsilon_1 = \omega - \omega_{ref} \\ \varepsilon_2 = \phi - \phi_{ref} \end{vmatrix}\right\rangle \quad \varepsilon = \begin{bmatrix} \varepsilon_1 \\ \varepsilon_2 \end{bmatrix} \quad (23)$$

ϕ_{ref}: is the flux reference; ω_{ref}: the rotor speed reference.

The differential equations governing the sliding mode are given by [3,5,8]:

$$\left.\begin{vmatrix} s_1 = \dot{\varepsilon}_1 + k_a\ \varepsilon_1 \\ s_2 = \dot{\varepsilon}_2 + k_b\ \varepsilon_2 \end{vmatrix}\right\rangle S = \begin{bmatrix} s_1 \\ s_2 \end{bmatrix} \quad (24)$$

k_a and k_b ensure the stability of the system when it is in sliding mode.

The derivative compared to the time of the sliding surface will be imposed by the system of equations according to [8]

$$\begin{cases} \dfrac{ds_1}{dt} = -\delta_1 \left(s_1 + \gamma_1 \; sign\left(s_1\right)\right) \\ \dfrac{ds_2}{dt} = -\delta_2 \left(s_2 + \gamma_2 \; sign\left(s_2\right)\right) \end{cases} \tag{25}$$

With δ_1, γ_1, δ_2 and γ_2 are positive constants in order to ensure the stability of the system. Indeed to ensure the sliding of the system at the time of its first passage by surface $S(X) = 0$ and to ensure the stability of the system, we consider the following function of Lyapunov:

$$V\left(X\right) = \frac{1}{2} S^t S \tag{26}$$

Its differential in relation to time is:

$$\begin{aligned} &\dot{V}\left(X\right) = S^t S \\ &\dot{V}\left(X\right) = -\left\{\delta_1 s_1^2 + \delta_2 s_2^2 + \delta_1 \gamma_1 \left|s_1\right| + \delta_2 \gamma_2 \left|s_2\right|\right\} < 0 \quad \Leftrightarrow \quad S\left(X\right) < 0 \end{aligned} \tag{27}$$

To determine the expression of the equivalent order, one calculates the derivative of the sliding surface while basing oneself on the expression, which gives [7], [9] and [12]:

$$f_1 = i_{sd}\varphi_{rd} + \; i_{sq}\varphi_{rq};\; f_2 = i_{sq}\varphi_{rd} - i_{sd}\varphi_{rq};\; f_3 = i_{sd}^2 + \; i_{sq}^2; \phi = \varphi_{rd}^2 + \; \varphi_{rq}^2 \tag{28}$$

Then the following matric form is obtained:

$$\begin{bmatrix} \dot{s}_1 \dfrac{1}{\sigma_7} \\ \dot{s}_2 \dfrac{t_r}{2} \end{bmatrix} = [F] + [D] \begin{bmatrix} u_{sd} \\ u_{sq} \end{bmatrix} \tag{29}$$

with

$$[F] = \begin{bmatrix} F_1 \\ F_2 \end{bmatrix}$$

$$F_1 = \left(a_1 + a_6 + k_a\right) f_2 - \omega \; f_1 - a_4 \omega \; \phi + \frac{a_8}{a_7}\left(k_a C_r - \dot{C}_r\right) - \frac{a_8}{a_7}\left(k_a C_f + \dot{C}_f\right) \tag{30-b}$$

$$-\frac{1}{a_7}\left(k_a \dot{\omega}_{ref} + \ddot{\omega}_{ref}\right)$$

$$F_2 = \left(\frac{T_r}{2}K_b - 1\right)\dot{\phi} - \frac{T_r}{2}\left(\ddot{\phi}_{ref} + K_b\dot{\phi}_{ref}\right) + M_{sr}\left(a_1 + a_6\right) f_1 + M_{sr}\omega f_2 + M_{sr}a_5 f_3 + M_{sr}a_3\,\phi \quad \textbf{(30-b)}$$

$$[D] = \begin{bmatrix} -b_1\varphi_{rq} & b_1\varphi_{rd} \\ M_{sr}\,b_1\varphi_{rd} & M_{sr}\,b_1\varphi_{rq} \end{bmatrix}$$

As the initial value of $\varphi_{rq} \neq 0$, the matrix *D* is regular. Hence, at the sliding mode, the equivalent control part can be obtained as:

$$U_{eq} = -[D]^{-1}[F] \quad \textbf{(31)}$$

Thus the determination of the nonlinear control part U_{nl} is related to the reaching condition; it is governed by [8]:

$$U_{nl} = -[D]^{-1}\begin{bmatrix} u_{01}\ \mathrm{sgn}(s_1) \\ u_{02}\ \mathrm{sgn}(s_2) \end{bmatrix} \text{with} \begin{cases} u_{01} > |F_1| \\ u_{02} > |F_2| \end{cases} \quad \textbf{(32)}$$

The shape of the control is given by:

$$U = U_{eq} + U_{nl} \quad \textbf{(33)}$$

4. Observer Design

You he electrical behavior of an induction motor can be described in the *(α;β)* coordinate system in stationary reference frame fixed with the stator. Under the assumption that the dynamic of the load torque is bounded, the induction motor model [22] is given by the following set of state variables equations:

$$\begin{cases} \dot{I} = KF(\omega)\psi - \gamma I - \dfrac{1}{L_s}U \\ \dot{\psi} = -F(\omega)\psi + \dfrac{M}{T_r}I \end{cases} \quad \textbf{(34)}$$

Where

$$I = \begin{bmatrix} i_{sa} & i_{sb} \end{bmatrix}^T; \psi = \begin{bmatrix} \varphi_{ra} & \varphi_{rb} \end{bmatrix}^T; U = \begin{bmatrix} u_{s\alpha} & u_{s\beta} \end{bmatrix}^T;$$

$$F(\omega) = \frac{1}{\tau_r}I_2 - n_{pp}\omega J_2;\ I_2 = \begin{bmatrix} 1 & 0 \\ 0 & 1 \end{bmatrix} and\ J_2 = \begin{bmatrix} 0 & -1 \\ 1 & 0 \end{bmatrix}$$

Where *I*, *Ψ*, *U* are respectively the stator current, the rotor fluxes and the voltage; ω denote the motor speed; The parameters *K* and γ are defined as follows:

$$\gamma = \frac{1}{\sigma\tau_s} + \frac{1-\sigma}{\sigma\ \tau_r};\ K = \frac{M_{sr}}{\sigma L_s\, L_r} \quad \textbf{(35)}$$

The measured output vector is $[I,\omega]^T$. A high gain observer which allows the estimation of y can be synthesized [**22**] and its equations are:

$$\begin{cases} \dot{\hat{I}} = KF(\omega_{mes})\hat{\psi} - \gamma\hat{I} - \dfrac{1}{\sigma L_s}U - 2\theta\left(\hat{I} - I\right) \\ \dot{\hat{\psi}} = -F(\omega_{mes})\hat{\psi} + \dfrac{M}{\tau_r}\hat{I} - \dfrac{\theta^2}{K}F^{-1}(\omega_{mes})\left(\hat{I} - I\right) \end{cases} \quad \textbf{(36)}$$

Where $\hat{I}$ and $\hat{\psi}$ are the respective estimates of I, Ψ and $\theta > 0$ is a design parameter.

5. Simulation Results

The simulated structure of the global system is given by the following figure5.

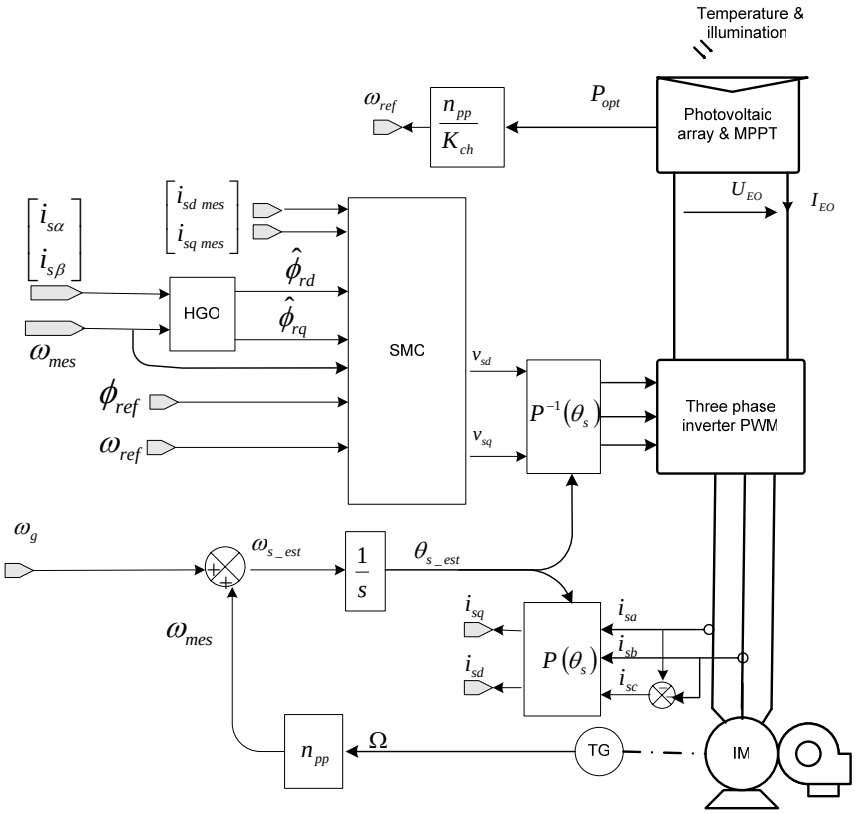

Fig. 5. Sliding mode control structure of an induction motor pump fed by a PVG

Within the framework of our application, the parameters of simulations are:

Table II : The three-phase induction motor-driven pump characteristic		
P_u =1Kw	L_s=0.5821H	F_v=0.004Nm/rad/s
N=1440tr/min	L_r=0.5821H	n_{pp}=2
R_s=8.87Ω	f_t=3500Hz	K_{ch}= 8.0197*10^{-5}
R_r=6.95Ω	J=0.01Kgm^2	M_{sr}=0.55452H
k_a= 450et k_b=700	u_{01}= u_{02}=2.5	θ=1

All simulations are carried with MATLAB 7.5. The results are illustrated by figures 6-13 respectively.

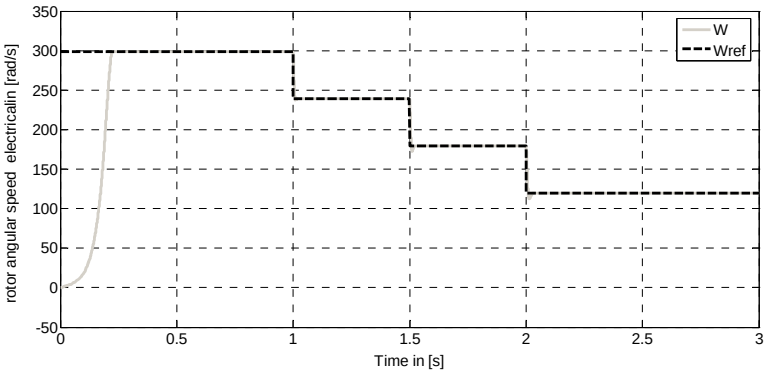

Fig.6. Mechanical speed and the corresponding reference signal

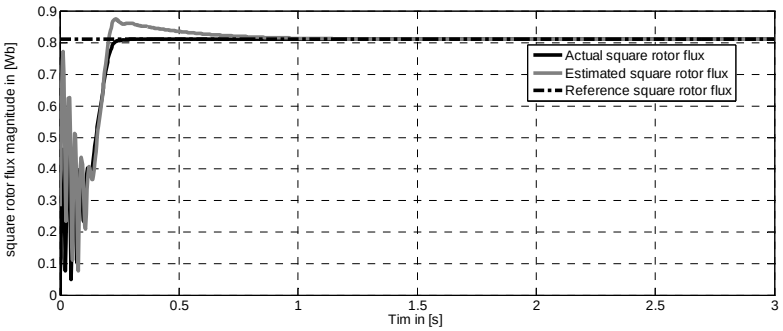

Fi g.7. Actual, estimated and reference square rotor flux

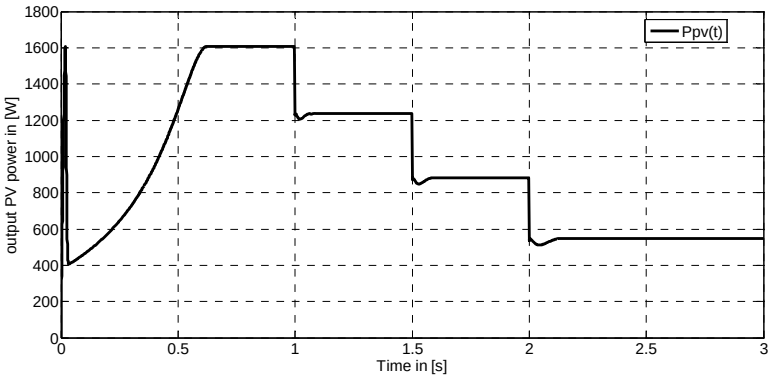

Fig.8. Output of the PV power

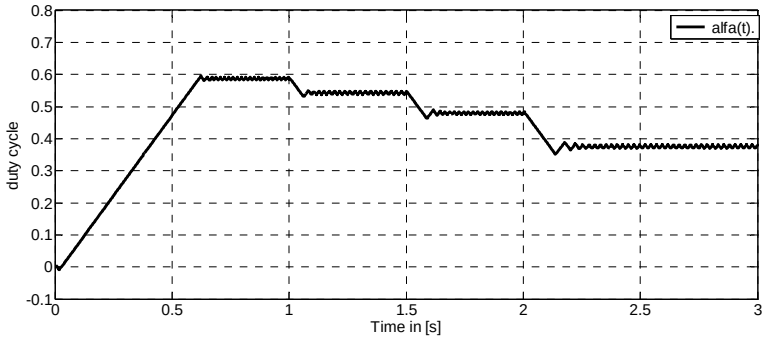

Fig.9. Duty cycle of the DC-DC boost converter

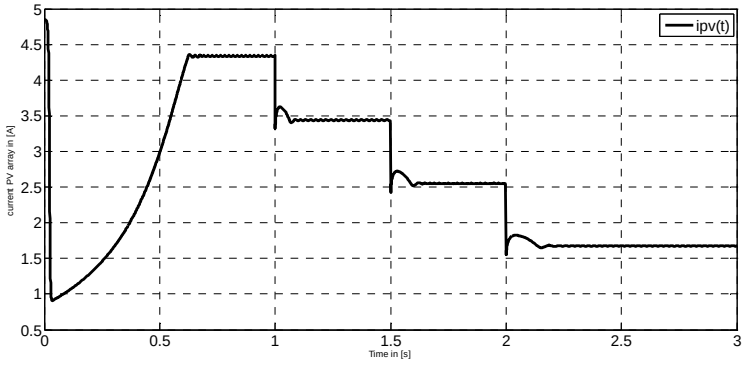

Fig.10. Current output of the PVG

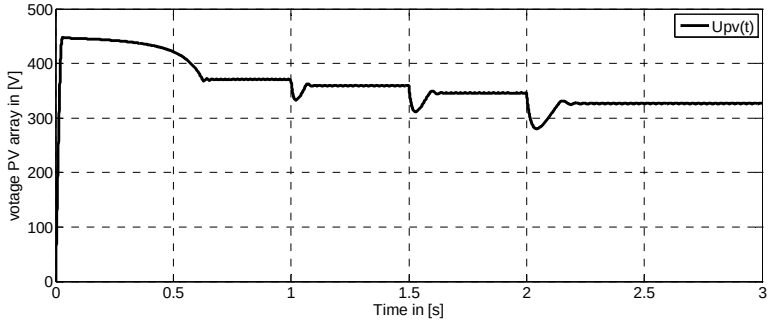

Fig.11. Voltage output of the PVG

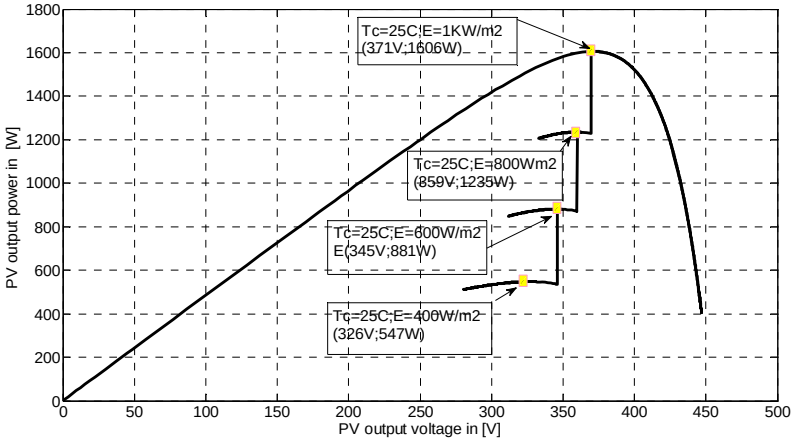

Fig. 12. Ppv(Upv) curves for several irradiation conditions

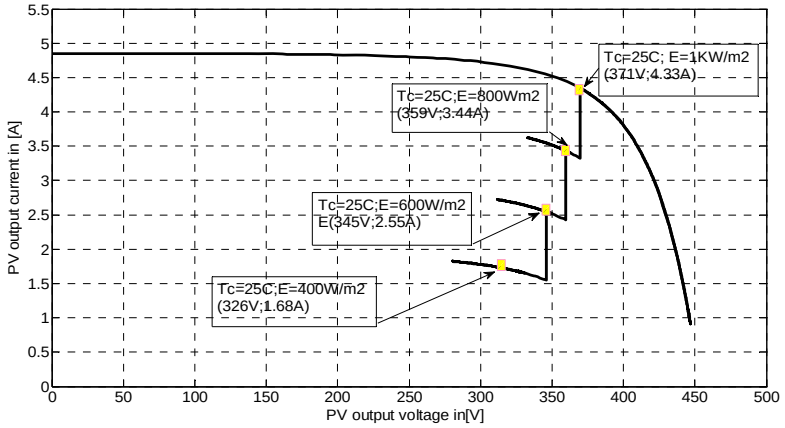

Fig. 13. Ipv(Upv) curves for several irradiation conditions

The simulation results show that:

- The square one of rotor flow ϕ tends asymptotically towards its value of reference 0.81Wb;
- The electric speed of rotor ω reaches its value of reference;
- The performances of the observer are illustrated in figure 9 where the estimation error on ϕ is less than 1.5%.

6. Conclusion

The modeling of the induction motor-driven pump group supplied with a PVG, shows well that this type of system has nonlinearities, Indeed, PVG is characterized by non linearity of its electric characteristic and its dependence on the climatic conditions. Therefore, it can not be comparable with any other traditional generator of electric power of continuous type. In this case, we suggest using a variable structure control with sliding mode which belongs to robust control approaches that treat nonlinear systems. High gain observers have been used in order to provide the missing states used by the control laws.

We presented the steps to be followed for the application of the sliding mode control SMC to an induction motor driven pump coupled to a PVG.
Simulations results which are presented show the performances of the SMC in order to force the PVG to work at its maximum power point. The developed SMC assures the convergence at the same time of the electric speed of rotor and the square module of rotor flux towards their reference values.

References

[1] I. S. Kim, M. B. Kim, and M. J. Youn, “New maximum power point tracker using sliding-mode observer for estimation of solar array current in the grid-connected photovoltaic system,” IEEE Trans. Ind. Electron, vol. 53, no. 4, pp. 1048–1054, Aug. 2006.

[2] Bahgat.A.B.G, Helwab.N.H, Ahmad.G.E and El Shenwyb.T: "Maximum power point tracking controller for PV systems using neural networks", Renewable Energy. Vol. 30, pp. 1257–1268, 2005.

[3] Hua.C and Latin.J" An on-line MPPT algorithm for rapidly changing illuminations of solar arrays "Renewable Energy, pp1129-1142, 2003.

[4] Trishan E and Patrick L: " Comparison of Photovoltaic Array Maximum Power Point Tracking Techniques" IEEE Transactions on Energy Conversion, Vol. 22, NO. 2, June 2007, pp439-449.

[5] L. Wu, Z. Zhao and J. Liu, “A single-stage three-phase grid-connected photovoltaic system with modified MPPT method and reactive power compensation,” IEEE Transactions on Energy Conversion, Vol. 22, No. 4, pp. 881-886, 2007.

[6] S. Liu and R. A. Dougal, “Dynamic multiphysics model for solar array,” IEEE Trans. Energy Convers., vol. 17, no. 2, pp. 285–294, Jun. 2002.

[7] S Rauschenbach, “ Solar cell Array Design Handbook, Van Nostrand Reinhold company, 1980.

[8] K.H. Hussein, I. Muta, T. Hoshino, M. Osakada, “Maximum Power Point Tracking: an algorithm for rapidly changing atmospheric conditions”, IEE proccedings of Generation, Transmission and Distribution, vol. 142, no. 1, Jan. 1995.

[9] G. Hanifi, “Sliding Mode Control of Dc-Dc Boost Converter”, Journal of Applied Sciences 5(3):588-592, 2005.

[10] K. Chomsuwan, P. Prisuwanna, et al., “Photovoltaic grid-connected inverter using two-switch buck boost converter,” in Conf. Rec. 2002 IEEE Photovoltaic Specialists Conf., pp. 1527-1530, May 2002.

[11] W. Xiao, W.G. Dunford, "A modified adaptive hill climbing MPPT method for photovoltaic power systems," in Conf. Rec. 2004 IEEE Annu. Power Electronics Specialists Conf.(PESC'04), vol.3, pp. 1957-1963, Jun. 2004.

[12] T. Noguchi, S. Togashi, et al., "Short-current pulse based maximum-power-point tracking method for multiple photovoltaic- and-converter module system," IEEE Trans. Ind. Electron., vol. 49, pp. 217-223, Feb. 2002.

[13] C. Hua, C, Shen, "Comparative study of peak power tracking techniques for solar storage systems," in 1998 Proc. IEEE Applied Power Electronics Conf. and Expo., (APEC'98), pp. 697-685, 1998.

[14] N. Patcharaprakiti, S. Premrudeepreechacharn, "Maximum power point tracking using adaptive fuzzy logic control for grid-connected photovoltaic system," presented at the IEEE Power Engineering Society Winter Meeting, vol.1, pp. 372-377, Jan. 2002.

[15] A. Torres, F. Antunes, F. Reis, "An artificial neural network-based real time maximum power tracking controller for connecting a PV system to the grid," in 1998 Proceeding, IEEE Annual Conf. Industrial Electronics Society (IECON'98), vol.1, pp. 554-558, Aug.-Sept. 1998

[16] EsramT, Chapman PL. Comparison of photovoltaic array maximum power point tracking methods. IEEE Transactions on Energy Conversion June 2007;22(2).

[17] Liu X, Lopes LAC. An improved perturbation and observation maximum power point tracking algorithm for PV arrays. IEEE 35th Annual Power ElectronicsSpecialists Conference, PESC 04 20–25 June 2004;3:2005–10.

[18] Yu GJ, Jung YS, Choi JY, Kim GS. A novel two-mode MPPT control algorithm based on comparative study of existing algorithms. Solar Energy April 2004;76(4):455–63.

[19] H.A. Toliyat, E. Levi, M. Raina, A review of RFO induction motor parameter estimation techniques, IEEE Trans. Energy Conversion 18 (2003)

[20] A. Benchaib, A. Rachid, E. Audrezet, and M. Tadjine, "Real-time sliding mode observer and control of an induction motor," IEEE Trans. Ind. Electron., vol. 46, no. 1, pp. 128–138, Feb. 1999.

[21] Benchaib.A, Rachid.A and Audrez.E: "Sliding Mode Input Output Linearisation and Field Orientation For Real Time Control of Induction Motors", IEEE Trans, Power Electronics. Vol 14, no.1, pp3 -13, January 1999.

[22] Jean-François, Philippe Dorléans, Sofien Hajji, Mohammed M'Saad and Mondher Farza "High-gain-based output feedback controllers for the induction motor," SSD 07 vol. 1, March 19-22, 2007, Hammamet, Tunisia